Bioactive Materials 10 (2022) 355–366

Contents lists available at ScienceDirect

Bioactive Materials

journal homepage: www.sciencedirect.com/journal/bioactive-materials

A functional PVA aerogel-based membrane obtaining sutureability through modified electrospinning technology and achieving promising anti-adhesion effect after cardiac surgery

Dawei Jin [a,1], Shuofei Yang [b,1], Shuting Wu [a], Meng Yin [a,*], Haizhu Kuang [c,**]

[a] Department of Cardiothoracic Surgery, Shanghai Children's Medical Center, School of Medicine, Shanghai Jiao Tong University, 1678 Dong Fang Road, Shanghai, 200127, People's Republic of China
[b] Department of Vascular Surgery, Renji Hospital, School of Medicine, Shanghai Jiao Tong University, 160 Pujian Road, Shanghai, 200127, People's Republic of China
[c] Department of Pharmacy, The Third Affiliated Hospital (The Affiliated Luohu Hospital) of Shenzhen University, Shenzhen, 518001, Guangdong Province, People's Republic of China

ARTICLE INFO

Keywords:
Anti-Adhesion
PVA aerogel-Based membrane
Sutureability
Modified electrospinning technology
Pericardial reconstruction

ABSTRACT

Pericardial barrier destruction, inflammatory cell infiltration, and fibrous tissue hyperplasia, trigger adhesions after cardiac surgery. There are few anti-adhesion materials that are both functional and sutureable for pericardial reconstruction. Besides, a few studies have reported on the mechanism of preventing pericardial adhesion. Herein, a functional barrier membrane with sutureability was developed via a modified electrospinning method. It was composed of poly(L-lactide-*co*-caprolactone) (PLCL) nanofibers, poly(vinyl alcohol) (PVA) aerogel, and melatonin, named PPMT. The PPMT had a special microstructure manifested as a staggered arrangement of nanofibers on the surface and a layered macroporous aerogel structure in a cross-section. Besides providing the porosity and hydrophilicity obtained from PVA, the structure also had suitable mechanical properties for stitching due to the addition of PLCL nanofibers. Furthermore, it inhibited the proliferation of fibroblasts by suppressing the activation of *Fas* and *P53*, and achieved anti-inflammatory effects by affecting the activity of inflammatory cells and reducing the release of pro-inflammatory factors, such as interleukin 8 (IL-8) and tumor necrosis factor α (TNF-α). Finally, *in vivo* transplantation showed that it up-regulated the expression of matrix metalloproteinase-1 (MMP1) and tissue inhibitor of metalloproteinase-1 (TIMP1), and down-regulated the expression of Vinculin and transforming growth factor β (TGF-β) in the myocardium, thereby reducing the formation of adhesions. Collectively, these results demonstrate a great potential of PPMT membrane for practical application to anti-adhesion.

1. Introduction

Tissue adhesions are the most common postoperative complication of surgical operation [1]. Surgical handling, tissue exposure, bleeding, and inflammation are all related to the formation of adhesions [2]. Depending on the location, the organs involved, and the severity, it can further lead to related sequelae, such as chronic pain or intestinal obstruction after abdominal surgery [3], infertility after pelvic surgery [4], and abnormal limb movements after orthopedic surgery [5]. Reducing surgical operations could help prevent adhesion formation [6,7]. However, for most congenital heart diseases, usually characterized by structural malformations of the heart and abnormal connections of blood vessels, a staged surgery and an extensive anatomical dissection in the narrow mediastinum is necessary [8,9]. Therefore, pericardial adhesion after cardiac surgery is theoretically inevitable without proper treatment, leading to unclear anatomical boundaries. It further results in a longer dissection time and a higher probability of bleeding events during the staged operations. Pericardial adhesions can also restrict the left ventricular diastolic filling even without reoperation. This decreases the left ventricular stroke volume and causes sudden death in severe

Peer review under responsibility of KeAi Communications Co., Ltd.
* Corresponding author.
** Corresponding author.
E-mail address: mengyinmdphd@shsmu.edu.cn (M. Yin).
[1] Dawei Jin and Shuofei Yang contributed equally to this work.

https://doi.org/10.1016/j.bioactmat.2021.08.013
Received 1 July 2021; Received in revised form 1 August 2021; Accepted 7 August 2021
Available online 19 August 2021

cases [10].

The intact pericardium acts as a barrier between the myocardium and external tissues, thereby reducing adhesion formation [11,12]. However, it is often cut and used to re-establish normal blood circulation (sealing the ventricular septal defect or enlarging narrowed arteries) during the treatment of congenital heart diseases [13]. Meanwhile, postoperative adhesion is excessive hyperplasia of scar tissue, including the infiltration of inflammatory cells and the proliferation of fibrocytes [12,14]. Therefore, an ideal anti-adhesion material should meet the needs of surgical operations, anti-fibrosis, and anti-inflammatory [15,16]. Various products, including sprays, hydrogels, and membranes, have been used to prevent tissue adhesions [17–22]. However, only a few functional anti-adhesion materials can be used for pericardial reconstruction since a few materials can meet all the three requirements above [23–25].

Herein, a functional and sutureable anti-adhesion membrane PPMT, composing of PLCL nanofibers, PVA aerogel, and melatonin was developed. As two commonly used biomaterials [26], PLCL nanofibers enhances the mechanical properties of composite materials to ensure the sutureability [27]. PVA aerogel is macroporous and highly hydrophilic, providing a good drug loading system and a certain anti-adhesion effect based on material science [28,29]. Furthermore, melatonin, a hormone secreted by the pineal gland, regulates the circadian rhythm, but it has other roles. In recent years, other biological effects of melatonin, such as the anti-inflammatory and anti-fibrosis effects, have been explored. Melatonin deficiency can promote inflammatory cell recruitment and induce excess fibrous tissue formation, thus causing the formation of adhesions [30,31]. Therefore, the traditional electrospinning method was modified to manufacture a functional barrier membrane with the superior characteristics of PLCL nanofibers and PVA aerogel to the greatest extent. Meanwhile, both *in vitro* and *in vivo* experiments were conducted to demonstrate its effect and potential mechanism of anti-pericardial adhesion.

2. Materials and methods

2.1. Preparation of barrier membranes

PLCL (Daigang Biotechnology Co., Ltd., China) with an L-lactic acid/e-caprolactone ratio of 50:50 was dissolved in 1,1,1,3,3,3-hexafluoro-2-propanol (HFIP, Darui Fine Chemical Co., Ltd., China) at a concentration of 20% to create the spinning solution. Melatonin (0.2g) (M5250, Sigma-Aldrich, USA) was dissolved in 2 ml of 75% alcohol solution, then 18 ml of water was added. PVA (1.6g) with a viscosity of 20.0–30.0 mPa s (Mackin Biochemical Co., Ltd., China) was added to the melatonin solution and stirred. The PVA/melatonin solution was then put into a rectangular iron box, and the prepared PLCL spinning solution was connected to a high-voltage power supply through a 10 mL syringe. The PLCL nanofibers were then directly spun into the PVA/melatonin solution at 1.0 mL/h and 12–15 kV for 1–1.5 h. The PVA/melatonin solution mixed with PLCL nanofibers was put into a fridge at a constant temperature of −80 °C for 24 h, then thawed at room temperature for 12 h. The freeze-thaw process was repeated thrice then the sample was dried for 12 h. Finally, a drug-loaded membrane was obtained, and it was named PPMT.

PLCL nanofiber membrane was obtained by receiving PLCL nanofibers, PVA aerogel membrane by repeatedly freeze-thawing the pure PVA solution thrice, and PLCL/PVA membrane (PP) by spinning the PLCL nanofibers into PVA solution without melatonin. All these procedures followed the above conditions.

2.2. Characterizations of barrier membranes

2.2.1. Morphology observation

The above-prepared materials were cut into equal-sized squares, then sprayed with gold for 30 s (twice). The microstructure of different membranes was then observed using an S-4800 (Hitachi) scanning electron microscope at an accelerating voltage of 10 kV. Both surface and cross-section images were obtained.

2.2.2. Porosity calculation

The porosity of different membranes was calculated as previously described [32]. First, a certain mass (recorded as M_0) of dry samples was put into distilled water at room temperature for 48 h. The surface moisture was then removed by putting samples on absorbent tissue, and the samples were immediately weighed (M_1). The samples were then placed in distilled water, and their mass re-weighed (M_2). The volume density of the sample was calculated as follows:

$$\rho_b\left(g/cm^3\right) = \rho_w * M_0/[M_1 - M_2] \quad (1)$$

ρ_w is the density of water at room temperature.

Second, the membranes were cut into long samples (3 cm × 1 cm), and their thickness was measured using a micrometer (an accuracy of 0.01 mm). For each sample, three different positions were measured, then averaged. Finally, the apparent density (ρ_a) and porosity (P) of different membranes were calculated using formulas (2) and (3) as follows:

$$\rho_a\left(g/cm^3\right) = (g)/\left[d(cm) \times (cm)^2\right] \quad (2)$$

m, d and S represent the quality, thickness, and area of membranes.

$$P = \left[1 - \rho_a\left(g/cm^3\right)/\rho_b\left(g/cm^3\right)\right] \times 100\% \quad (3)$$

2.2.3. Drug loading confirmation and release evaluation

Fourier transform infrared spectroscopy (FTIR, Nicolet 6700, Thermo Scientific, USA) was used to confirm the drug loading of PPMT membrane, at room temperature in the range of 4000–1000 cm^{-1} at a resolution of 4.0 cm^{-1}, and the number of runs was 32 times. In addition, the UV spectrophotometer (UV-1900, Shimadzu, Japan) was used to evaluate the drug release of PPMT. Firstly, the standard curve of melatonin was drawn based on its characteristic absorption peak at a wavelength of 278 nm. Briefly, PPMT membrane (0.2g) was immersed in a 15 mL centrifuge tube containing 10 mL PBS solution. The tube was incubated in a horizontal continuous shaker at 37 °C and 120 cycles/min. Then, 3 mL of medium was collected to test by UV–vis spectrophotometer, and data was recorded. Then, the remainder medium was removed, and 10 mL of fresh PBS was added again for subsequent incubation at the prescheduled time. Both the drug released per day and the accumulated released amount curves were drawn.

2.2.4. Hydrophilicity test

A contact angle tester (OCA40, Dataphysics, German) was used to assess the hydrophilicity of different materials. Briefly, the materials were cut into the same shapes and put on coverslips. A 0.03 mL deionized water was put on the surface of the materials. The contact angle was then measured and recorded at the steady state of the droplets. At least three samples (random locations) of each group were measured and averaged.

2.2.5. Mechanical properties test

An Electro-Force 3200 testing machine (TA, USA) was used for the tensile and suture retention strength tests of different materials at room temperature. The linear elastic modulus was determined using the stress-strain curves.

Briefly, different barrier materials were cut into a rectangular shape (2 cm by 1 cm), and their thickness was measured using a spiral micrometer. The material was then fixed between two clamps at a distance of 2 mm and stretched at 0.2 mm/s to obtain the corresponding stress-strain curve. Each sample was pierced at 2 mm from the edge

using a 6–0 absorbable PDS II suture thread (Johnson & Johnson, NJ, USA) (same size as the one used for *in vivo* experiment) for the suture retention strength test. The suture and the edges of the material were fixed in two clamps. Tests were performed at 0.2 mm/s up to pull the suture through the material or cause the break of the sample. All the samples were fully soaked with PBS solution for 5 min before performing the above tests to simulate the watery environment *in vivo*.

2.3. In vitro anti-fibroblast evaluation

First, a Cell Counting Kit-8 (CCK-8) (Dojindo Lab., Japan) was used to detect the proliferation of fibroblasts (L929s). Briefly, the fibroblasts were cultured using different materials at 2×10^4 cells/well in Dulbecco's modified eagle's medium (DMEM) (Gibco, China) with 10% Fetal Bovine Serum (FBS) (Gibco, China) and 1% penicillin-streptomycin (Gibco, China) under the standard culture condition (37 °C and 5% CO_2). Blank coverslips were used as the controls. The medium was changed every two days. CCK-8 solution (400 μL) was added to each well after one, four, and seven days of culture, and cells were further incubated for another 2 h. A microplate reader (MK3, Thermo, USA) was used to measure the absorbance in each well at 450 nm. Meanwhile, the cells were stained with Rhodamine Phalloidin and DAPI (Yeasen Biotech Co., Ltd, China) after culturing for four days to observe the morphology using laser confocal microscopy (CLSM, Leica, USA).

A flow cytometer (Becton, Dickinson & Co., USA) was used to assess the detailed information of cell proliferation and division cycle. First, some fibroblasts were pre-labeled using Cell Proliferation Tracer Detection Kit (Beyotime Biotech Co., Ltd, China) following the protocols. The labeled cells were then seeded into different materials with at 1×10^5 cells/well. The cells were cultured at 37 °C and 5% CO_2 for 24 h, then digested for fluorescence intensity attenuation analysis of carboxyfluorescein succinimidylamino ester (CFSE). Besides, other untreated fibroblasts were seeded into different materials at an equal density of 1×10^5 cells/well and digested after 24 h of culture. The cells were labeled using a cell division cycle detection kit (Beyotime Biotech Co., Ltd, China) before cell division cycle detection.

Moreover, the *P53* and *Fas* genes were used to explore molecular changes in the mRNA and protein expression levels. Different materials were separately placed into a 6-well plate after sterilization. L929s were inoculated at 2.0×10^5 cells/well, and six parallel groups were set up. The cells were collected to extract the mRNA and protein after 24 h of culture.

2.4. In vitro anti-inflammatory evaluation

The anti-inflammatory effect of different materials was indicated by the proliferation of monocytes (THP-1) and the secretion of inflammatory factors. Meanwhile, the effects of different materials on the ability of monocytes to differentiate into macrophages were also evaluated. First, the sterilized materials were placed into a 24-well plate, and the monocytes were seeded at $4–5 \times 10^5$ cells/ml. PMA solution was then added to a final concentration of 100 ng/ml to stimulate monocyte differentiation. The macrophages were cultured in RPMI Modified Medium (Hyclone, USA) with 10% Fetal Bovine Serum (FBS) (Gibco, China) and 1% penicillin-streptomycin (Gibco, China) for 48 h. They were then stained with TRITC Phalloidin (MKbio, China) and DAPI (Yeasen Biotech Co., Ltd, China), and laser confocal microscopy (CLSM, Leica, USA) was used to observe the morphology.

Second, different materials were separately placed into a 6-well plate after sterilization. The pre-labeled monocytes were then inoculated in RPMI Modified Medium (Hyclone, USA) with 10% Fetal Bovine Serum (FBS) (Gibco, China) and 1% penicillin-streptomycin (Gibco, China) at $4–5 \times 10^5$ cells/ml, then cultured at 37 °C and 5% CO_2 for 48 h. Next, a flow cytometer (Becton, Dickinson & Co., American) was used to assess the fluorescence intensity attenuation. Other untreated monocytes were also seeded into different materials at an equal density, then cultured for 48 h. The cells were then labeled using a cell cycle and apoptosis analysis kit (Biosharp, China) before cell division cycle detection.

Furthermore, the inflammatory factors secreted by monocytes were detected using an ELISA kit (Labtache Technologies Co., Ltd, China). Briefly, monocytes were cultured following the above steps. The cell suspension was centrifuged at 1000×*g* for 5 min after 48 h of culture. The supernatant was then collected for IL-8, TGF-β, and TNF-α expression analyses.

2.5. In vivo anti-pericardial adhesion evaluation

2.5.1. Animal model and surgical interventions

A total of 36 New Zealand white rabbits underwent pericardial reconstruction surgery. All procedures followed the ARRIVE guidelines and were approved by the Animal Ethics Committees of Shanghai Children's Medical Center, Shanghai Jiaotong University. The experiments also followed the National Institutes of Health guide for the care and use of laboratory animals (NIH Publications No. 8023, revised 1978). The animals were divided into four groups, including the control group (without pericardial reconstruction), the PLCL, the PP, and the PPMT membrane groups. The postoperative follow-up time was one month, two months, and three months.

Briefly, anesthesia was induced via a slow intravenous injection of 3% sodium pentobarbital solution (1 ml/kg). The animals were then endotracheally intubated and mechanically ventilated at 15–18 breaths/min. The general anesthesia was maintained using a gas mixture of oxygen at 1.5 L/min and isoflurane at a concentration of 0.5%. The chest skin was prepared, and the thoracic cavity was opened, exposing the pericardium for defect creation. Different materials were then used to reconstruct the pericardium with several interrupted 6–0 polydioxanone synthetic (PDS II) absorbable suture threads (Johnson & Johnson, USA). The chest cavity was then closed. Pericardial reconstruction was not conducted on animals in the control group. Antimicrobial antibiotics were intramuscularly administered for one week. Postoperative pain was controlled using intramuscular buprenorphine (0.03 mg/kg).

2.5.2. Evaluation of immune response

The level of C-reactive protein (CRP), immunoglobulin G (IgG), immunoglobulin M (IgM), immunoglobulin A (IgA) and total immunoglobulin E (IgE) at 3 days after surgery was measured using Ottoman-1000 machine (UPPER, China) and SIEMENS specific protein analyzer (SIEMENS, German) respectively to evaluate the acute immune response. Briefly, 4 ml venous blood was collected from each rabbit, of which 2 ml was used for CRP testing and 2 ml for immunoglobulin testing. All procedures were performed strictly in accordance with the related kit instructions. The kits for inflammation evaluation were CRP-1006 (UPPER, China) and N LateX IgG/A/M/E mono (SIEMENS, German). The normal rabbits were used as control group and the values were averaged.

2.5.3. Cardiac function assessment

An echocardiographic system (Phillips CX50) with an S5-1 sector array transducer was used for transthoracic echocardiography to assess cardiac function. The short-axis M-mode images were presented, and dimensions of the left ventricle at both diastole (LVIDd) and systole (LVIDs) were measured. The ejection fraction (EF), fraction shortening (FS), and end-systole volume (ESV) were also calculated.

2.5.4. Pericardial adhesion grading

Pericardial adhesions were graded at the terminal time of follow-up. The left thoracotomy was used to evaluate the adhesion. The pericardium was exposed, then the adhesion score was assessed using a grading system as follows: 0 indicated no adhesions; 1 showed thin adhesions, with a foamy dissection plane; 2 showed intermediate adhesions, requiring some sharp dissection; and 3 indicated dense adhesions, which

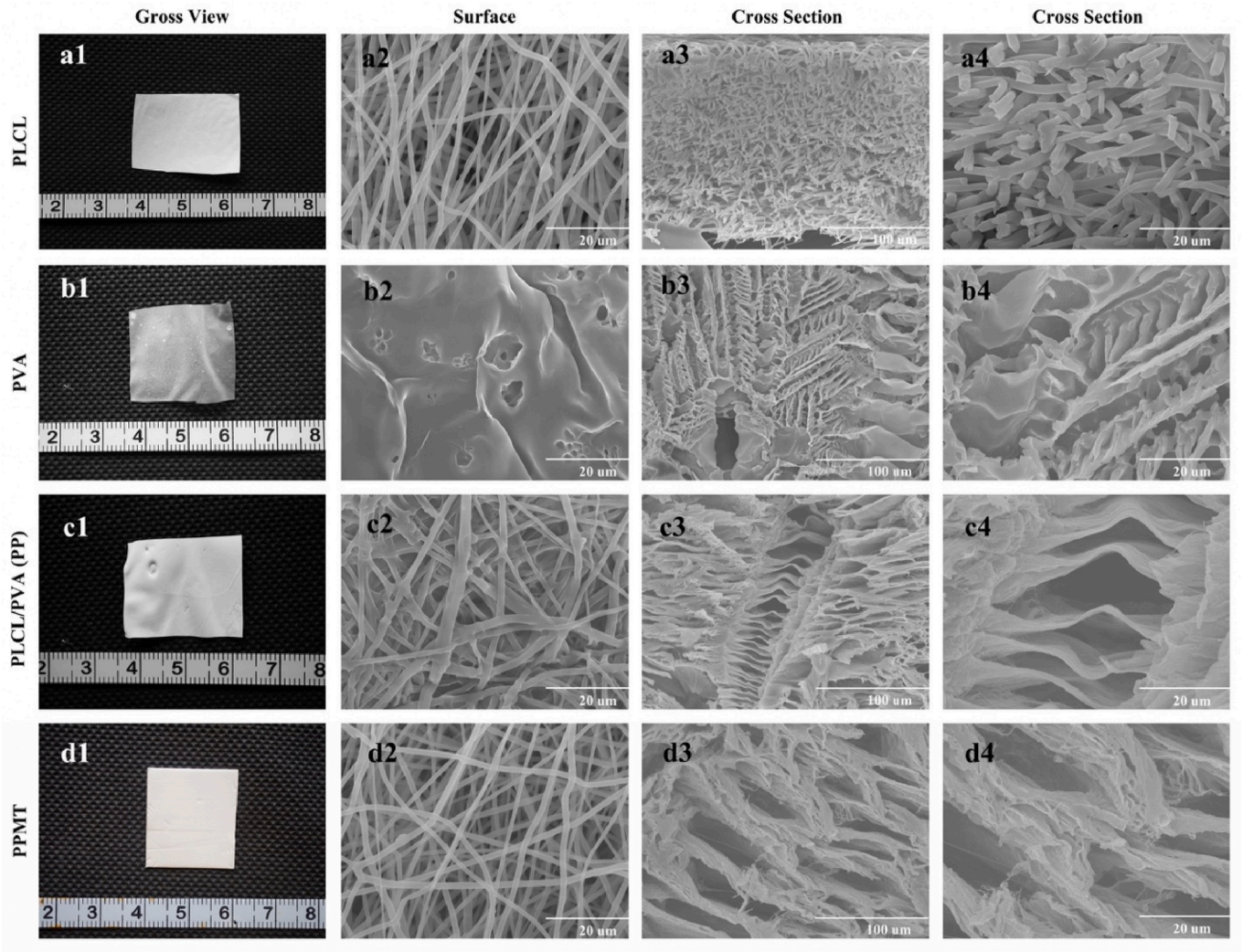

Fig. 1. Gross view and microstructure of different barrier membranes. (a1-d1) The digital images of PLCL, PVA, PLCL/PVA (PP) and PPMT. (a2-d2) The SEM images of surface. (a3-d4) The SEM images of cross-section.

can easily lead to bleeding, requiring exclusive sharp dissection. The adhesion scores were averaged for each group.

2.5.5. Tissue staining and protein expression analysis

The rabbits were anesthetized to death at each follow-up time point before harvesting the pericardial adhesion tissues and attached myocardium for tissue staining and protein expression analysis. Briefly, pericardial adhesion tissues were fixed in 4% formalin and embedded in paraffin. The sections (5 μm) were obtained for hematoxylin-eosin (H&E) and Masson trichrome staining.

Additionally, the myocardium was ground with liquid nitrogen in a mortar (tissues around the barrier membrane were harvested to perform the same procedure for rabbits without adhesions). The ground tissue (50 mg) was mixed with 300 μl of pre-cooled protein lysis solution (T-PER™, Thermo, USA) containing PMSF and protease inhibitors, then incubated on ice for 15 min. The mixture was then centrifuged at 10,000*g* to obtain supernatant. BCA (Pierce™ BCA Protein Assay Kit, Thermo, USA) was used for quantitative leveling, then loading buffer was added and boiled at 95–100 °C for 10 min. The protein was subjected to sodium lauryl sulfate polyacrylamide electrophoresis and transferred to a nitrocellulose membrane. The following antibodies were used: anti-*anti*-Vinculin (A2752), *anti*-TGF-β (A2407), *anti*-MMP1 (A0067), *anti*-TIMP1 (A1389) (ABclonal, China), and HRP-conjugated GAPDH (#HRP-60004) (Proteintech, USA). The samples were incubated with the primary antibodies at 4 °C overnight, then HRP-conjugated secondary antibody. The luminescence signal on the membrane was detected using electrochemiluminescence (Shanghai Share Biotechnology). Western blot images were obtained using the LAS4000 imaging system (Fujifilm, Canada), and band densitometry was quantified as arbitrary light units using ImageJ software.

2.6. Data analysis

All data were obtained from at least three parallel samples and are expressed as mean ± SD. GraphPad Prism 8.0 Software (GraphPad Software Inc, La Jolla, CA) was used for all statistical analyses. One-way ANOVA was used to evaluate the statistical differences between groups, and $p < 0.05$ was considered statistically significant.

3. Results and discussion

3.1. Characterizations of barrier membranes

Electrospinning technology is widely used to prepare drug-loaded medical materials [33–35]. In order to manufacture a functional membrane with the superior characteristics of PLCL nanofibers and PVA aerogel to the greatest extent, the traditional electrospinning method was modified. Both the PP and PPMT membrane had a special

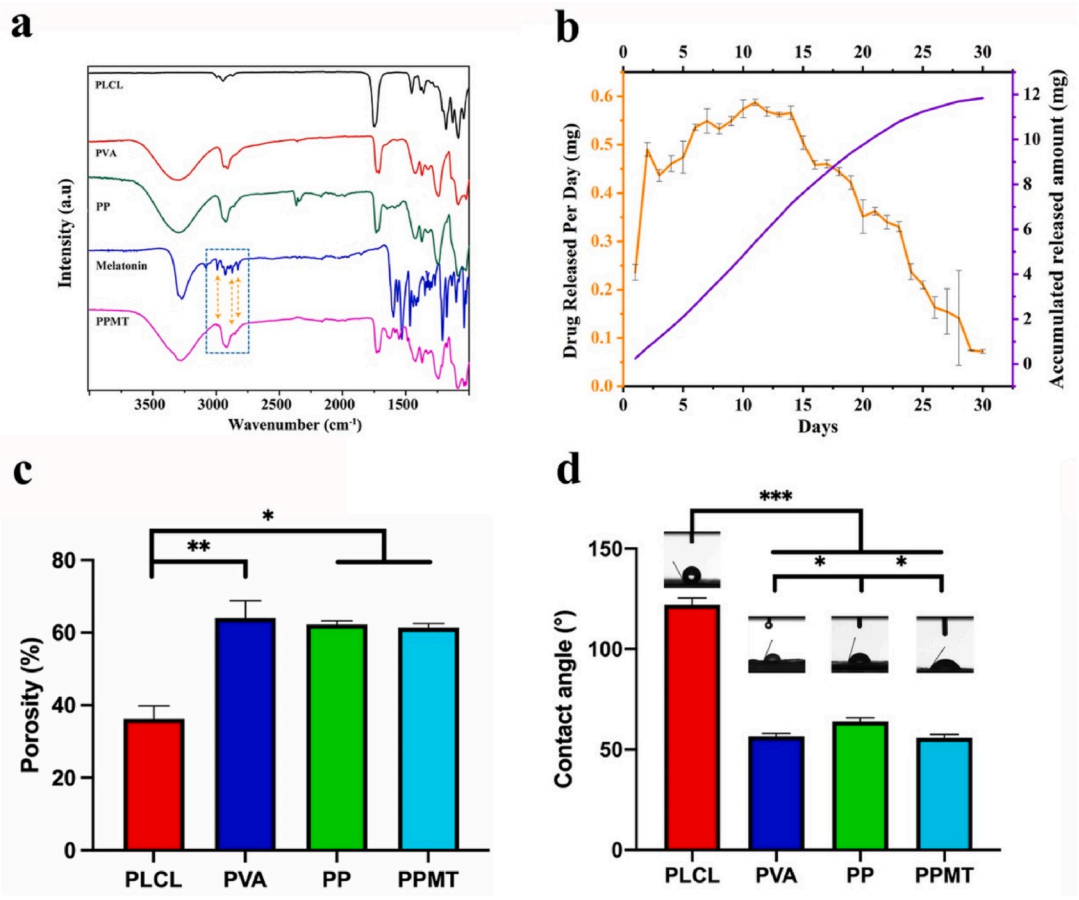

Fig. 2. Characterizations of different barrier membranes. (a) The infrared spectroscopy analysis. (b) The drug release evaluation. (c) The statistical comparison of porosity. (d) The statistical comparison of contact angle.

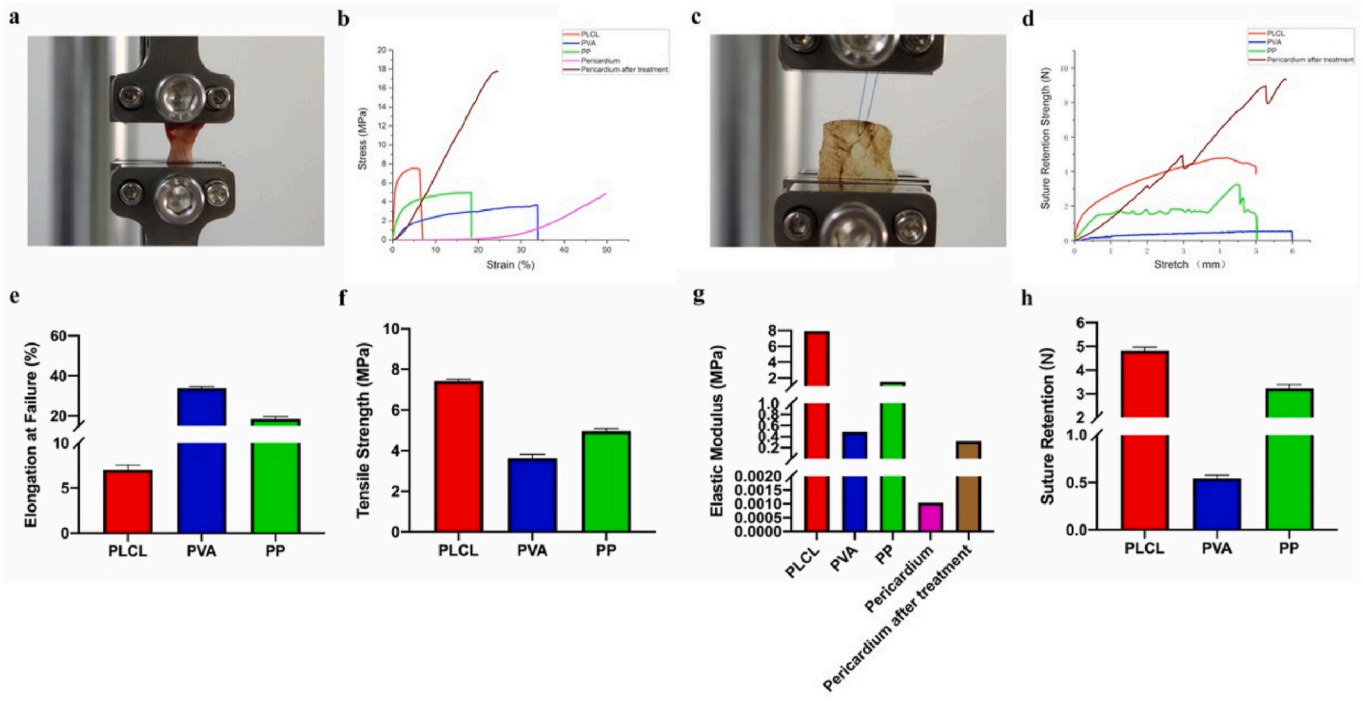

Fig. 3. Mechanical properties of different membranes. (a) Schematic diagram of tensile test. (b) Curves of strain-stress. (c) Schematic diagram of suture retention strength test. (d) Curves of suture retention strength. (e) Maximum elongation of different materials. (f) Tensile strength of different materials. (g) Elastic modulus of different materials. (h) Suture retention strength of different materials.

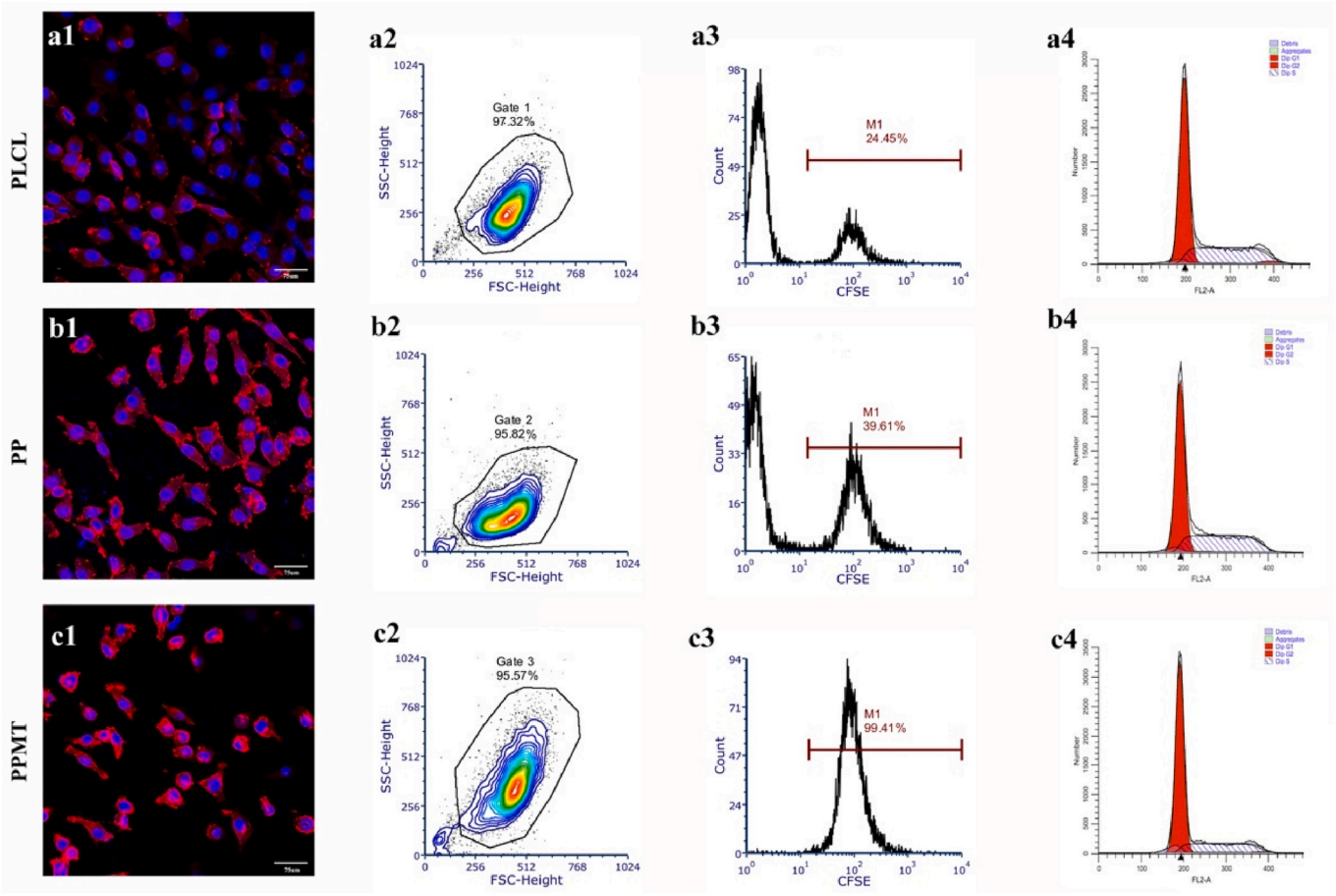

Fig. 4. The morphology and proliferation of fibroblasts. (a1-c1) Rhodamine staining photomicrograph of L929s on PLCL, PP, PPMT after four days of culturing. (a2-c2) Cell population of L929s on PLCL, PP, PPMT after one day of culturing. (a3-c3) Flow cytometric analysis of cell proliferation of L929s on PLCL, PP, PPMT after one day of culturing. (a4-c4) Flow cytometric analysis of cell cycle of L929s on PLCL, PP, PPMT after one day of culture.

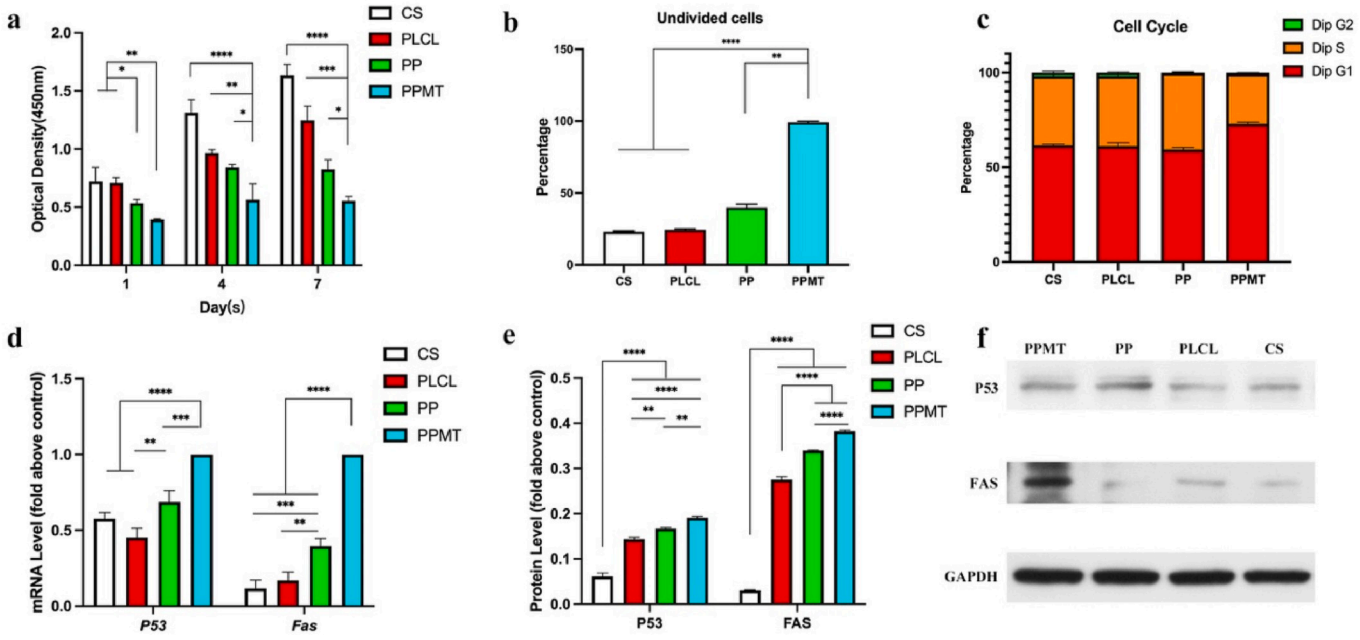

Fig. 5. The statistical analysis of fibroblasts proliferation and activity of *P53* and *Fas*. (a) The optical density of cell medium within one week of culture. (b) The percentage of undivided L929s after one day of culture. (c) The proportions of L929s in each interphase after one day of culture. (d) The mRNA transcription level of *P53* and *Fas* after one day of culture. (e) The protein expression level of *P53* and *Fas* after one day of culture. (f) Western blot image of *P53* and *Fas*.

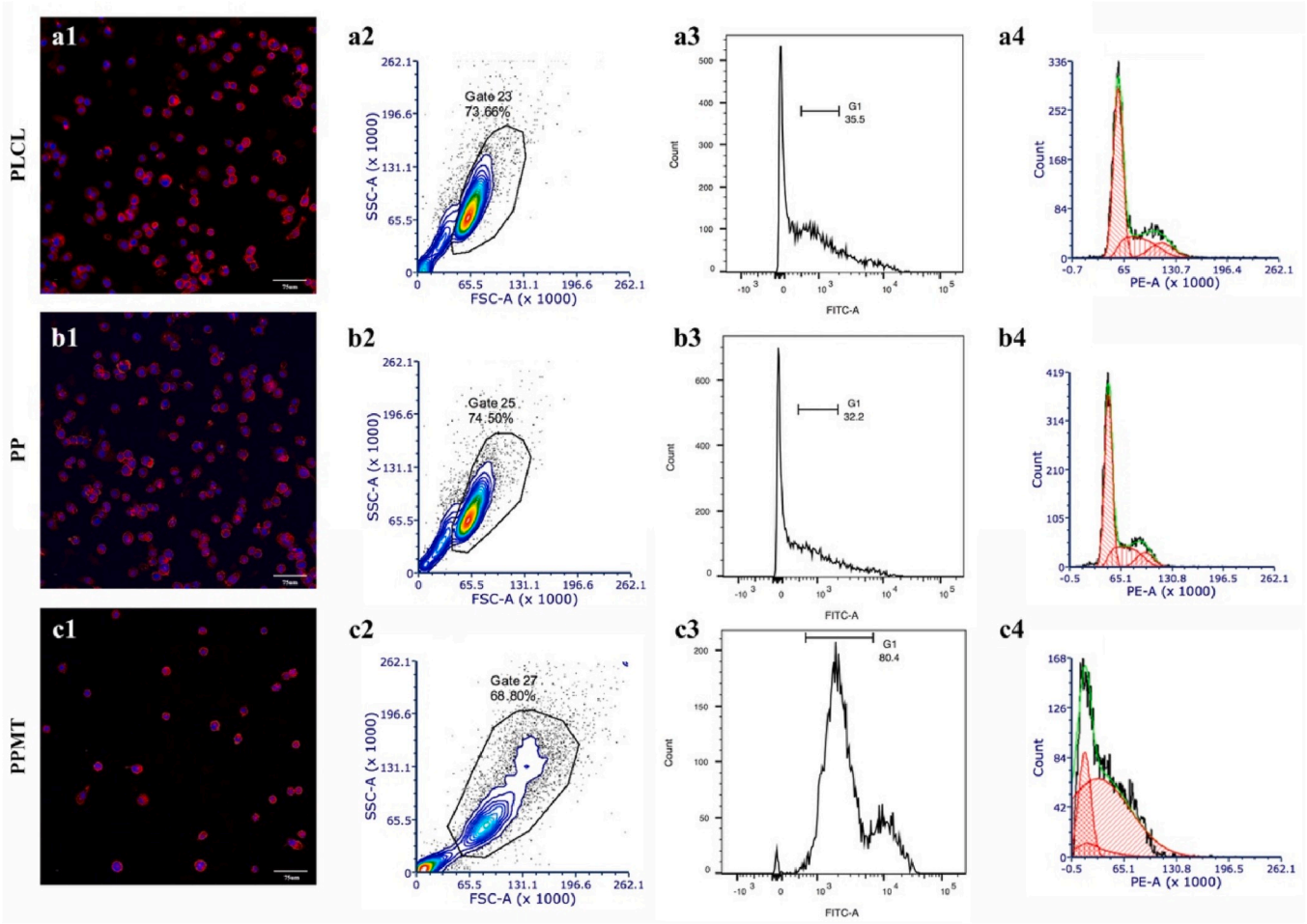

Fig. 6. The morphology of macrophages and proliferation of monocytes. (a1-c1) TRITC Phalloidin staining of macrophages on PLCL, PP, PPMT after 48 h of differentiation. (a2-c2) Cell population of THP-1 in PLCL, PP, PPMT after two days of culturing. (a3-c3) Flow cytometric analysis of cell proliferation of THP-1 in PLCL, PP, PPMT after two days of culturing. (a4-c4) Flow cytometric analysis of cell cycle of THP-1 in PLCL, PP, PPMT after two days of culture. (d–f) Release of representative pro-inflammatory factors: IL-8, TNF-α, TGF-β. (g) The proportions of THP-1 in each interphase on different materials.

microstructure, presenting staggered nanofibers on the surface like the PLCL membrane and layered macro-porous structure in the cross-section similar to the PVA aerogel membrane (Fig. 1(a2-d4)). These could enhance its mechanical strength, porosity, and hydrophilicity, providing sutureability and indicating its use as an ideal drug loading platform [36,37]. The loading of melatonin was confirmed through the infrared spectroscopy analysis, with a visualization of PPMT membrane and melatonin sharing multiple similar characteristic peaks at 2750–3100 nm (Fig. 2a). Meanwhile, the melatonin in the PPMT membrane could be released continuously for one month, during which the daily release amount gradually increased in the first 15 days, and then showed a downward trend in the second half month. In terms of the cumulative release over time, it presented the characteristics of sustained release, showing a smooth curve (Fig. 2b). Additionally, the porosity between PVA, PP, and PPMT membranes was not statistically different, all of which were higher than that of PLCL membrane (Fig. 2c). Besides, as shown in Fig. 2d, the PVA, PP, and PPMT membranes all showed better hydrophilicity than the PLCL membrane (122.1° ± 3.361°). Although there was a slight increase in contact angle of PP membrane (63.97° ± 1.750°) compared with PVA membrane, it was decreased with the addition of melatonin. The contact angle between PVA (56.60° ± 1.320°) and PPMT membranes (55.88° ± 1.596°) was not statistically different, indicating that PPMT and PVA membranes have similar hydrophilicity.

3.2. Mechanical properties of barrier membranes

The mechanical properties of barrier membrane determine whether it can meet pericardium replacement and surgical operations requirements. As the clothing of the heart, the applied barrier membrane needs a suitable tensile strength and elasticity to withstand about 50,000–10,000 heartbeats per day. Meanwhile, a strong suture retention strength is also needed for anastomoses. Herein, the tensile and suture retention strength tests were conducted for different materials. The autologous porcine pericardium was employed as a control before and after glutaraldehyde fixation (Fig. 3a and c).

The untreated porcine pericardium had excellent elongation, and its mechanical properties underwent significant changes after fixation (Fig. 3b), making it more suitable for surgical operation (Fig. 3d). Although the PVA aerogel membrane had greater elongation and a closer elastic modulus to fixed porcine pericardium compared with the PLCL and PP membrane (Fig. 3e and g), it had the least tensile strength (Fig. 3f) with almost no suture retention strength (Fig. 3h), indicating that the PVA membrane cannot withstand great tension and be used in surgical operations. With the addition of PLCL nanofibers, the prepared PP membrane had moderate elongation at break, similar tensile strength to the PLCL membrane and similar elasticity to the PVA membrane (Fig. 3e-g). More importantly, the suture retention strength of the PP membrane was significantly improved compared with the PVA membrane (Fig. 3h), indicating its suitability of stitching.

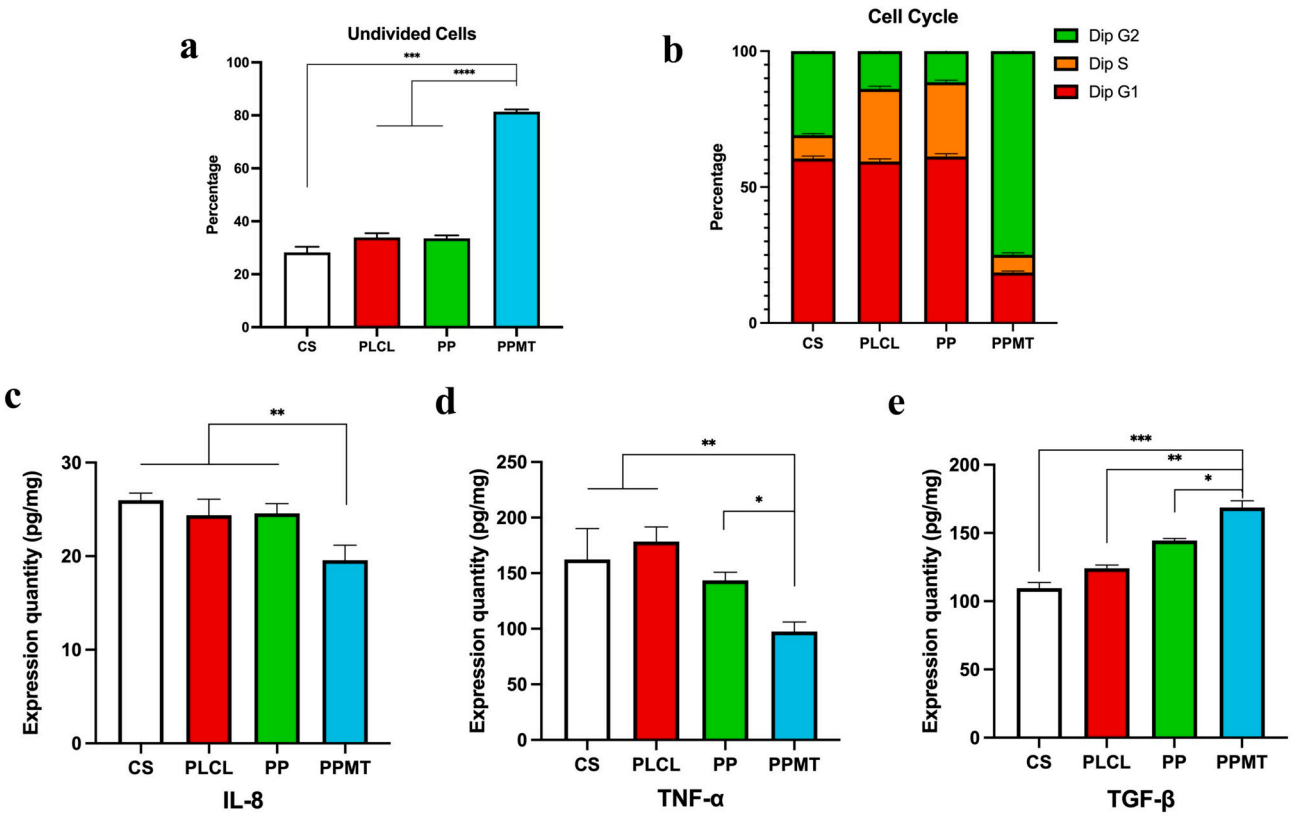

Fig. 7. The statistical analysis of monocytes proliferation and release of inflammatory factors. (a) The percentage of undivided THP-1 after two days of culture. (b) The proportions of THP-1 in each interphase after two days of culture. (c–e) Release of representative inflammatory factors: IL-8, TNF-α, TGF-β.

Table 1
The level of CRP and immunoglobulin of rabbits.

	Normal	Control	PLCL	PP	PPMT
CRP (mg/L)	< 1	< 1	< 1	< 1	< 1
IgG (mg/mL)	< 1.35	< 1.35	< 1.35	< 1.35	< 1.35
IgA (mg/mL)	< 0.07	< 0.07	< 0.07	< 0.07	< 0.07
IgM (mg/mL)	< 0.18	< 0.17	< 0.17	< 0.17	< 0.17
Total IgE (IU/mL)	< 18.20	< 18.20	< 18.20	< 18.20	< 18.20

3.3. *In vitro anti-fibroblast performance*

Adhesive tissue is mostly composed of fibrous tissue, and fibroblasts are essential for its formation. Therefore, inhibiting fibroblast proliferation can effectively prevent the occurrence of postoperative adhesion [38]. The confocal imaging showed that different from the spindle-shaped structure on the PLCL membrane and PP membrane, the fibroblasts were round-like on the PPMT membrane, suggesting the activity of fibroblasts might be affected (Fig. 4(a1-c1)). Furthermore, the flow cytometric analysis showed that most fibroblasts on the PPMT membrane did not undergo cell division and proliferation after 24 h of culture (the time required for one generation of division), showing no attenuation of the fluorescence intensity of CFSE (Fig. 4c3). However, different proportions of fibroblasts on the PLCL and PP membranes had completed a generation of mitosis, which manifested as different degrees of CFSE fluorescence intensity attenuation (Fig. 4a3, 4b3). The cell cycle is the process from the end of the parental cell division to the end of the progeny cell division of cells that proliferate in a mitotic manner. Generally, the proliferation ability is determined by the proportion of cells in the S phase. Compared with the PLCL and PP membrane, fewer fibroblasts were in the S phase on the PPMT membrane (Fig. 4a4-4c4), suggesting that the PPMT membrane can inhibit fibroblast proliferation.

The CCK-8 test showed that the proliferation rate of fibroblasts was slowest on the PPMT membrane (Fig. 5a). To be detailed, the proportion of undivided fibroblasts on the PPMT membrane after 24 h of culture was up to 99.08% ± 0.7757%, which was significantly higher than other groups. By contrast, the proportion of undivided fibroblasts on the PLCL and PP membrane was 39.76% ± 2.563% and 24.38% ± 0.6630%, respectively (Fig. 5b). Additionally, the proportion of fibroblasts in the S phase on the PPMT membrane was 26.28% ± 0.8253%, which was lower than that of the PLCL and PP membrane (Fig. 5c). *P53* and *Fas* regulate cell proliferation and apoptosis. *Fas* induces cell apoptosis, while *P53* inhibits proliferation and division by preventing cells in the G1 phase from entering the S phase [39–43]. This study explored the potential molecular mechanism of PPMT membrane on inhibiting fibroblasts proliferation using the level of mRNA transcription and protein expression of *P53* and *Fas*. The *P*53 and *F*as gene of fibroblasts were more active on three materials with a distinguishingly higher mRNA transcription and protein expression level on different membranes than the blank control group (Fig. 5d-f). Overall, the above results indicate that various membranes have different anti-fibroblast abilities, strongest in the PPMT membrane.

3.4. *In vitro anti-inflammatory performance*

Adhesion is the body's excessive repair of tissue damage to some extent. Besides the aforementioned role of fibroblasts, they are also involved with the recruitment and activation of inflammatory cells [44, 45]. Therefore, the anti-inflammatory effect of different materials was evaluated via the proliferation and differentiation of monocytes and the inflammatory factors secretion. Fewer monocytes on the PPMT membrane differentiated into macrophages compared with those on PLCL and PP membranes (Fig. 6a1-6c1), indicating that the PPMT membrane can cause less local tissue inflammation. Furthermore, flow cytometric analysis was used to determine monocyte proliferation in different

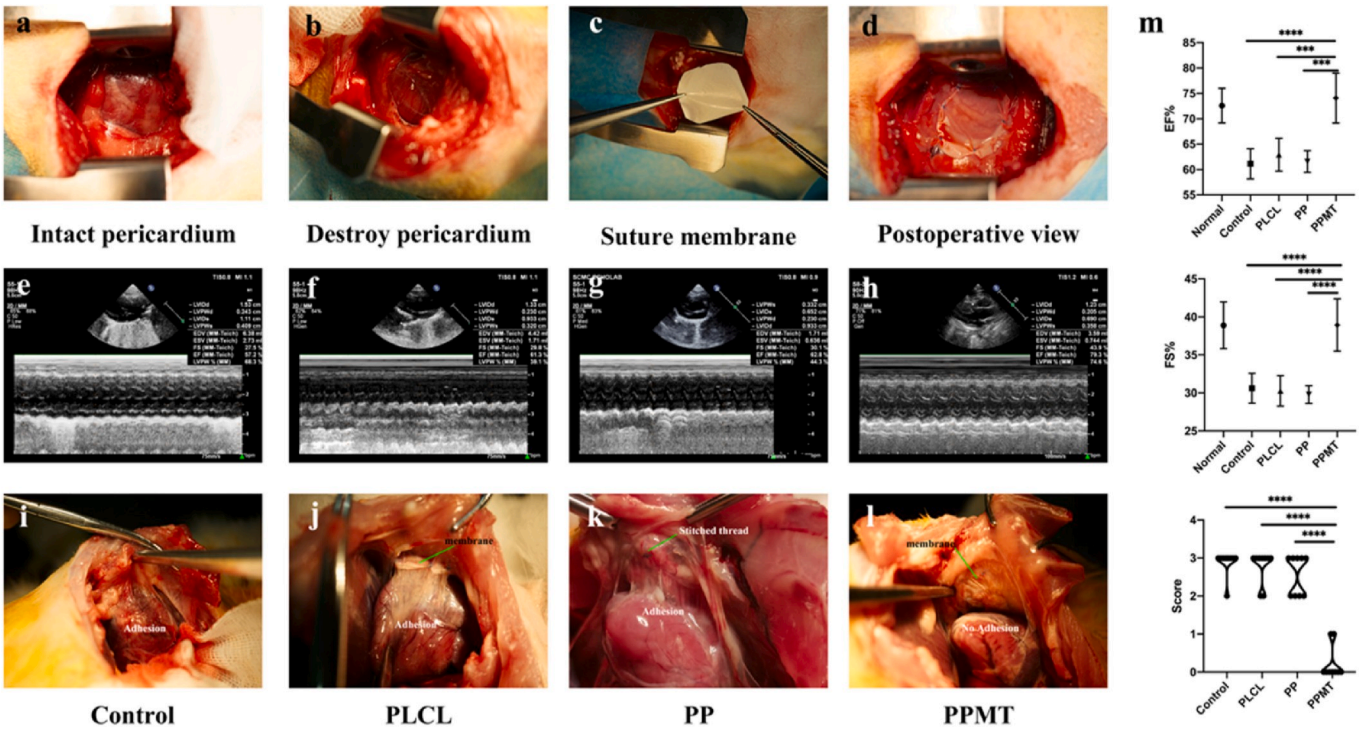

Fig. 8. Surgical interventions and postoperative performance of different materials. (a–d) Surgical operations. (e–h) Representative echocardiograms of postoperative animals after three months of transplantation. (i–l) Representative adhesion after three months of transplantation. (m) The statistics of EF, FS and adhesion score after three months of transplantation.

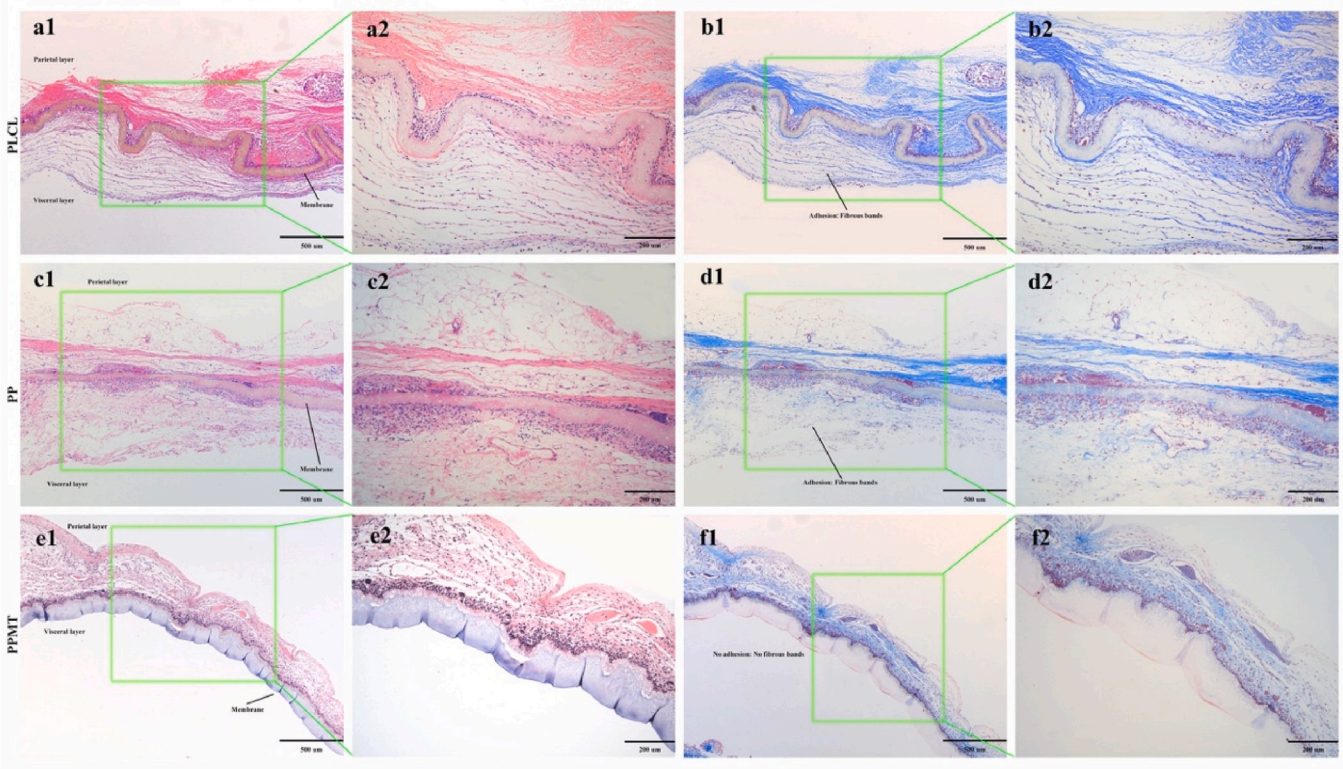

Fig. 9. Tissue staining three months after transplantation: H&E staining of PLCL (a1, a2), PP (c1, c2), PPMT (e1, e2) group and Masson staining of PLCL (b1, b2), PP (d1, d2), PPMT (f1, f2) groups under different magnifications.

materials. Like fibroblasts, the PPMT membrane also inhibited monocyte proliferation, manifested as slower attenuation of CFSE fluorescence intensity (Fig. 6a3-6c3). However, different from fibroblasts, the monocytes in the PPMT group were significantly affected (Fig. 6a2-6c2). Statistically, the proportion of undivided monocytes in the PPMT group after two days of culture was up to 81.37% ± 0.8737%, significantly

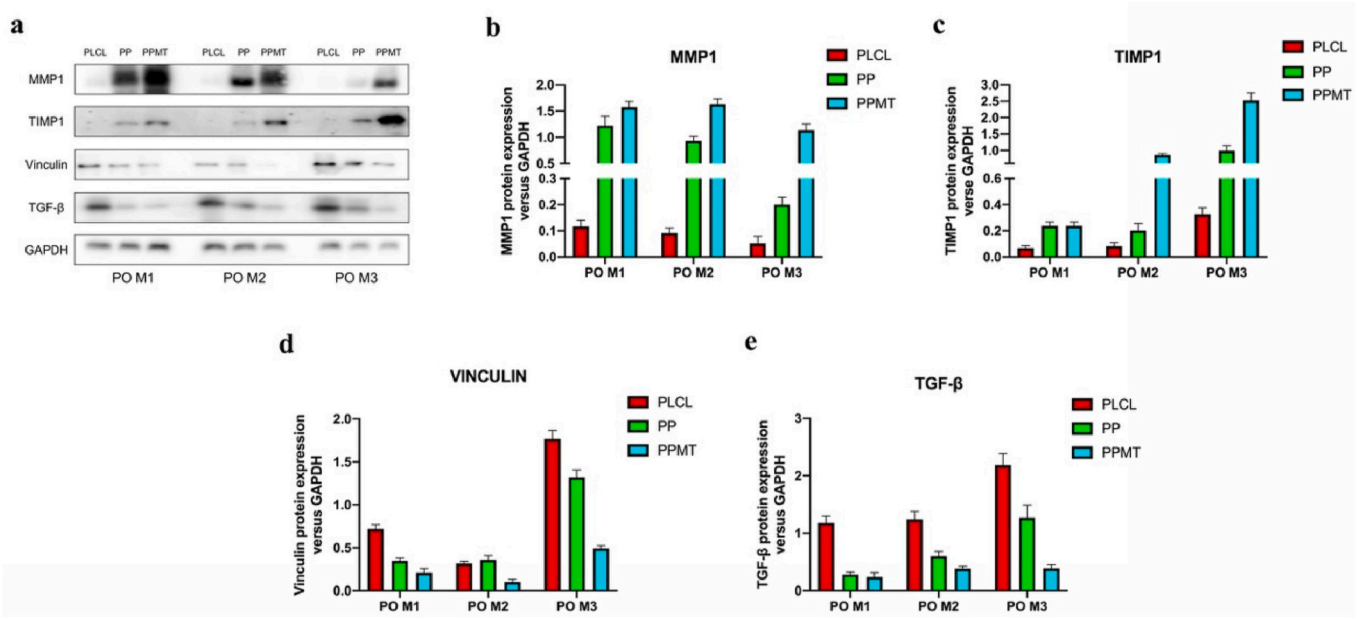

Fig. 10. Pro-adhesion and anti-adhesion protein expressions of harvested tissues in different groups. (a) Western blot image of proteins during the follow-up. (b–e) Each protein expression versus GAPDH during the follow-up.

higher than that of the PLCL and PP group, which was 33.90% ± 1.600% and 33.47% ± 1.168%, respectively (Fig. 7a). DNA content of the PPMT group was significantly reduced compared with that of PLCL and PP groups (Fig. 6a4-6c4), indicating fewer polyploid cells in the S phase. The cell cycle analysis showed that more monocytes were in the G2 phase (Fig. 7b), indicating the impairment of the continuity and coordination of the normal cell cycle. DNA damage activated the cell cycle checkpoint to prevent damaged cells from entering the mitotic phase, thereby producing the block of the G2 phase and providing enough time for repairing [46,47].

Activated monocytes-macrophages produce IL-8 and TNF-α. IL-8 attracts and activates neutrophils [48–50], and TNF-α promotes T lymphocytes to secrete inflammatory factors, thereby strengthening the inflammatory response of local tissues [51–53]. Besides, TGF-β inhibits the proliferation of immunocompetent cells and the secretion of some pro-inflammatory cytokines (TNF-α and IFN-γ) [54–56]. The monocytes in the PPMT group secreted fewer IL-8 and TNF-α and more TGF-β than that of PLCL and PP group (Fig. 7c-e), indicating that the PPMT membrane had a certain anti-inflammatory effect.

3.5. Surgical interventions and postoperative performance

The human body is a highly enclosed system based on immunology. The body activates a cascade of immune responses, which is more complex than *in vitro* experiments against any foreign invasion [57,58]. This could explain why some products with good performance *in vitro* often fail to meet expectations after transplantation *in vivo*. Herein, all surviving rabbits were tested for inflammatory indicators in blood on the third day after surgery. As shown in Table 1, there was no detectable inflammatory response, meaning that none of the three materials caused rejection. All experimental rabbits survived till the end of the follow-up except for two rabbits (one in the positive control group and the other in the PLCL group) who died of unexplained diarrhea.

Suturing prepared membranes to native pericardium via the traditional interrupted suture method was successful (Fig. 8a-d). The barrier membranes fitted well on the surrounding tissues in the aqueous environment of the body, thereby preventing direct contact between the external tissues and myocardium. Indicators of cardiac function are often used to assess the severity of pericardial adhesions. Generally, adhesions around the myocardium can cause ventricular insufficiency, decreasing ejection fraction (EF) and fractional shortening (FS). During the follow-up, the animals in the PPMT group had the highest average value of EF and FS, which were both close to that of the normal rabbits (Fig. 8e-h) and significantly different from that of the PLCL and PP group (Fig. 8m).

In addition, the dissection of the rabbits at the end of the follow-up showed that the rabbits in the control groups had different degrees of postoperative adhesions, which were manifested by the formation of dense fibrous tissue between the myocardium and pericardium. However, no pericardial adhesion occurred in rabbits in the PPMT group. Both the surface of the myocardium and the visceral layer of the membrane were smooth and clean (Fig. 8i–l). The comparative statistics of adhesion scores are shown in Fig. 8m.

3.6. Protein expression and tissue staining

The tissue staining results showed that various barrier membranes caused different histological changes after transplantation. Different degrees of fiber strands were formed on the visceral layer of PLCL and PP membranes, consistent with the postoperative anatomy results. In contrast, there were no attached cells or tissues on the visceral layer of the PPMT membrane (Fig. 9), indicating that the PPMT membrane has an anti-fibroblast effect *in vivo*. Interestingly, the anti-adhesion effect of the PPMT membrane mainly occurred on its visceral layer, consistent with previous literature [59], indicating that fibroblasts or myofibroblasts from myocardium could be the dominant factors that drive pericardial adhesion formation [60–62].

Therefore, the myocardium connecting to adhesive tissue was harvested to analyze some proteins involved in extracellular matrix deposition and focal adhesion formation. The analysis sought to assess the mechanism of the PPMT membrane acting on myocardium to reduce pericardial adhesion. The MMP/TIMP pathway is involved in regulating the homeostasis of the extracellular matrix. The MMPs family degrades various protein components of the extracellular matrix, and the TIMPs family inhibits and regulates the function of the MMPs family [63–65]. The protein expression of MMP1 and TIMP1 was higher in the myocardium of the PPMT group than in that of PLCL and PP groups, suggesting that the PPMT can activate the MMP/TIMP pathway through the release of melatonin, thereby degrading tissue adhesion that occurs after the operation (Fig. 10b and c). Besides, during the follow-up, the

expression level of TIMP1 protein gradually increased, suggesting that the hydrolysis of MMPs on adhesion tissue is strongest in the early postoperative. Moreover, Vinculin was expressed in cells and extracellular matrix, playing an important role in cell adhesion and movement [66,67]. Vinculin expression was lowest in the PPMT group (Fig. 10d). Interestingly, the effect of different barrier membranes on TGF-β was inconsistent between cardiomyocytes *in vivo* and monocytes *in vitro* (Figs. 10e and 7e). Notably, TGF-β has multiple effects, including inhibiting inflammatory cells and promoting fibroblasts and extracellular matrix [68]. This inconsistency indirectly indicates that inhibiting cardiac fibroblasts can prevent pericardial adhesions.

4. Conclusion

Herein, a functional PVA aerogel-based membrane with suturability, PPMT, has been developed through a modified electrospinning method. This membrane has a special microstructure, presenting staggered nanofibers on the surface like the PLCL membrane and layered macro-porous structure in the cross-section similar to the PVA aerogel membrane. Its mechanical properties are comparable to autologous pig pericardium due to the addition of PLCL nanofibers, which is more effective than pure PLCL membrane and PVA aerogel. It also showed anti-fibroblast and anti-inflammatory effects by inhibiting the proliferation and activity of corresponding cells. Finally, *in vivo* experiments demonstrated that the PPMT membrane is more effective after surgery since it influences the anti-adhesion protein and pro-adhesion protein expression. Overall, the results imply that the PPMT membrane can be used as an anti-pericardial adhesion.

Declaration of competing interest

The authors declare no competing financial interests in this work.

CRediT authorship contribution statement

Dawei Jin: Conceptualization, Performing experiments, Data analysis, Writing original draft. **Shuofei Yang:** Methodology, Writing original draft. **Shuting Wu:** Performing experiments. **Meng Yin:** Supervision, Funding acquisition, Writing – review & editing. **Haizhu Kuang:** Investigation, Resources, Writing – review & editing.

Acknowledgements

The National Natural Science Fund of China (81873923) and Shanghai Science and Technology Development Fund (20Y11910600, 18441901900) supported this study.

References

[1] M.P. Diamond, M.L. Freeman, Clinical implications of postsurgical adhesions, Hum. Reprod. Update 7 (6) (2001) 567–576.
[2] M.P. Diamond, S.D. Wexner, G.S. diZereg, M. Korell, O. Zmora, H. Van Goor, M. Kamar, Adhesion prevention and reduction: current status and future recommendations of a multinational interdisciplinary consensus conference, Surg. Innovat. 17 (3) (2010) 183–188.
[3] V. Mais, Peritoneal adhesions after laparoscopic gastrointestinal surgery, World J. Gastroenterol. 20 (17) (2014) 4917–4925.
[4] W. Cates, T.M. Farley, P.J. Rowe, Worldwide patterns of infertility: is Africa different? Lancet 2 (8455) (1985) 596–598.
[5] A.S. Neviaser, J.A. Hannafin, Adhesive capsulitis: a review of current treatment, Am. J. Sports Med. 38 (11) (2010) 2346–2356.
[6] W.B. Robb, C. Mariette, Strategies in the prevention of the formation of postoperative adhesions in digestive surgery: a systematic review of the literature, Dis. Colon Rectum 57 (10) (2014) 1228–1240.
[7] D. Moris, J. Chakedis, A.A. Rahnemai-Azar, A. Wilson, M.M. Hennessy, A. Athanasiou, E.W. Beal, C. Argyrou, E. Felekouras, T.M. Pawlik, Postoperative abdominal adhesions: clinical significance and advances in prevention and management, J. Gastrointest. Surg. 21 (10) (2017) 1713–1722.
[8] R. Sun, M. Liu, L. Lu, Y. Zheng, P. Zhang, Congenital heart disease: causes, diagnosis, symptoms, and treatments, Cell Biochem. Biophys. 72 (3) (2015) 857–860.
[9] S. Kutty, M.L. Jacobs, W.R. Thompson, D.A. Danford, Fontan circulation of the next generation: why it's necessary, what it might look like, J Am Heart Assoc 9 (1) (2020), e013691.
[10] V.A. Ferraris, Pericardial adhesions and cardiac surgeons' nightmares, J. Thorac. Cardiovasc. Surg. 156 (4) (2018) 1609–1610.
[11] M. Jaworska-Wilczynska, P. Trzaskoma, A.A. Szczepankiewicz, T. Hryniewiecki, Pericardium: structure and function in health and disease, Folia Histochem. Cytobiol. 54 (3) (2016) 121–125.
[12] A. Fischer, T. Koopmans, P. Ramesh, S. Christ, M. Strunz, J. Wannemacher, M. Aichler, A. Feuchtinger, A. Walch, M. Ansari, F.J. Theis, K. Schorpp, K. Hadian, P.A. Neumann, H.B. Schiller, Y. Rinkevich, Post-surgical adhesions are triggered by calcium-dependent membrane bridges between mesothelial surfaces, Nat. Commun. 11 (1) (2020) 3068.
[13] A. Carotti, Surgical management of fallot's tetralogy with pulmonary atresia and major aortopulmonary collateral arteries: multistage versus one-stage repair, World J Pediatr Congenit Heart Surg 11 (1) (2020) 34–38.
[14] S.J. Marshall, S.C. Bayne, R. Baier, A.P. Tomsia, G.W. Marshall, A review of adhesion science, Dent. Mater. 26 (2) (2010) e11–e16.
[15] A. Cannata, D. Petrella, C.F. Russo, G. Bruschi, P. Fratto, M. Gambacorta, L. Martinelli, Postsurgical intrapericardial adhesions: mechanisms of formation and prevention, Ann. Thorac. Surg. 95 (5) (2013) 1818–1826.
[16] W. Wu, R. Cheng, J. das Neves, J. Tang, J. Xiao, Q. Ni, X. Liu, G. Pan, D. Li, W. Cui, B. Sarmento, Advances in biomaterials for preventing tissue adhesion, J. Contr. Release 261 (2017) 318–336.
[17] J.W. Burns, M.J. Colt, L.S. Burgees, K.C. Skinner, Preclinical evaluation of Seprafilm bioresorbable membrane, Eur. J. Surg. Suppl (577) (1997) 40–48.
[18] J.M. Seeger, L.D. Kaelin, E.M. Staples, Y. Yaacobi, J.C. Bailey, S. Normann, J. W. Burns, E.P. Goldberg, Prevention of postoperative pericardial adhesions using tissue-protective solutions, J. Surg. Res. 68 (1) (1997) 63–66.
[19] L. Li, N. Wang, X. Jin, R. Deng, S. Nie, L. Sun, Q. Wu, Y. Wei, C. Gong, Biodegradable and injectable in situ cross-linking chitosan-hyaluronic acid based hydrogels for postoperative adhesion prevention, Biomaterials 35 (12) (2014) 3903–3917.
[20] L.M. Stapleton, A.N. Steele, H. Wang, H. Lopez Hernandez, A.C. Yu, M.J. Paulsen, A.A.A. Smith, G.A. Roth, A.D. Thakore, H.J. Lucian, K.P. Totherow, S.W. Baker, Y. Tada, J.M. Farry, A. Eskandari, C.E. Hironaka, K.J. Jaatinen, K.M. Williams, H. Bergamasco, C. Marschel, B. Chadwick, F. Grady, M. Ma, E.A. Appel, Y.J. Woo, Use of a supramolecular polymeric hydrogel as an effective post-operative pericardial adhesion barrier, Nat Biomed Eng 3 (8) (2019) 611–620.
[21] S. Dhall, T. Coksaygan, T. Hoffman, M. Moorman, A. Lerch, J.Q. Kuang, M. Sathyamoorthy, A. Danilkovitch, Viable cryopreserved umbilical tissue (vCUT) reduces post-operative adhesions in a rabbit abdominal adhesion model, Bioact Mater 4 (1) (2019) 97–106.
[22] Z. Li, L. Liu, Y. Chen, Dual dynamically crosslinked thermosensitive hydrogel with self-fixing as a postoperative anti-adhesion barrier, Acta Biomater. 110 (2020) 119–128.
[23] S.M. Mayes, J. Davis, J. Scott, V. Aguilar, S.A. Zawko, S. Swinnea, D.L. Peterson, J. G. Hardy, C.E. Schmidt, Polysaccharide-based films for the prevention of unwanted postoperative adhesions at biological interfaces, Acta Biomater. 106 (2020) 92–101.
[24] C. Hu, F. Tang, Q. Wu, B. Guo, W.A. Long, Y. Ruan, L. Li, Novel trilaminar polymeric antiadhesion membrane prevents postoperative pericardial adhesion, Ann. Thorac. Surg. 111 (1) (2021) 184–189.
[25] M. Fujita, G.M. Policastro, A. Burdick, H.T. Lam, J.L. Ungerleider, R.L. Braden, D. Huang, K.G. Osborn, J.H. Omens, M.M. Madani, K.L. Christman, Preventing post-surgical cardiac adhesions with a catechol-functionalized oxime hydrogel, Nat. Commun. 12 (1) (2021) 3764.
[26] Y. Wang, Y. Zhao, L. Qiao, F. Zou, Y. Xie, Y. Zheng, Y. Chao, Y. Yang, W. He, S. Yang, Cellulose fibers-reinforced self-expanding porous composite with multiple hemostatic efficacy and shape adaptability for uncontrollable massive hemorrhage treatment, Bioact Mater 6 (7) (2021) 2089–2104.
[27] C.P. Laurent, C. Vaquette, X. Liu, J.F. Schmitt, R. Rahouadj, Suitability of a PLCL fibrous scaffold for soft tissue engineering applications: a combined biological and mechanical characterisation, J. Biomater. Appl. 32 (9) (2018) 1276–1288.
[28] M. Bashir, H.K. Syed, S. Asghar, M. Irfan, W.H. Almalki, S.A. Menshawi, I.U. Khan, P.A. Shah, I. Khalid, J. Ahmad, U.F. Gohar, K.K. Peh, M.S. Iqbal, Effect of hydrophilic polymers on complexation efficiency of cyclodextrins in enhancing solubility and release of diflunisal, Polymers 12 (7) (2020).
[29] P. Liu, H. Du, Z. Wu, H. Wang, J. Tao, L. Zhang, J. Zhu, Hydrophilic and anti-adhesive modification of porous polymer microneedles for rapid dermal interstitial fluid extraction, J. Mater. Chem. B 9 (27) (2021) 5476–5483.
[30] W. Hu, Z. Ma, S. Jiang, C. Fan, C. Deng, X. Yan, S. Di, J. Lv, R.J. Reiter, Y. Yang, Melatonin: the dawning of a treatment for fibrosis? J. Pineal Res. 60 (2) (2016) 121–131.
[31] J. Cipolla-Neto, F.G.D. Amaral, Melatonin as a hormone: New physiological and clinical insights, Endocr. Rev. 39 (6) (2018) 990–1028.
[32] F. Zheng, S. Wang, S. Wen, M. Shen, M. Zhu, X. Shi, Characterization and antibacterial activity of amoxicillin-loaded electrospun nano-hydroxyapatite/poly (lactic-co-glycolic acid) composite nanofibers, Biomaterials 34 (4) (2013) 1402–1412.
[33] V.S. Waghmare, P.R. Wadke, S. Dyawanapelly, A. Deshpande, R. Jain, P. Dandekar, Starch based nanofibrous scaffolds for wound healing applications, Bioact Mater 3 (3) (2018) 255–266.
[34] Y. Chen, M. Shafiq, M. Liu, Y. Morsi, X. Mo, Advanced fabrication for electrospun three-dimensional nanofiber aerogels and scaffolds, Bioact Mater 5 (4) (2020) 963–979.

[35] X. Zhang, S. Guo, Y. Qin, C. Li, Functional electrospun nanocomposites for efficient oxygen reduction reaction, Chem. Res. Chin. Univ. 37 (3) (2021) 379–393.
[36] M.S. Haider, M.M. Lübtow, S. Endres, S. Forster, V.J. Flegler, B. Böttcher, V. Aseyev, A.C. Pöppler, R. Luxenhofer, Think beyond the core: impact of the hydrophilic corona on drug solubilization using polymer micelles, ACS Appl. Mater. Interfaces 12 (22) (2020) 24531–24543.
[37] Q. Yao, J.G. Cosme, T. Xu, J.M. Miszuk, P.H. Picciani, H. Fong, H. Sun, Three dimensional electrospun PCL/PLA blend nanofibrous scaffolds with significantly improved stem cells osteogenic differentiation and cranial bone formation, Biomaterials 115 (2017) 115–127.
[38] D.S. Foster, C.D. Marshall, G.S. Gulati, M.S. Chinta, A. Nguyen, A. Salhotra, R. E. Jones, A. Burcham, T. Lerbs, L. Cui, M.E. King, A.L. Titan, R.C. Ransom, A. Manjunath, M.S. Hu, C.P. Blackshear, S. Mascharak, A.L. Moore, J.A. Norton, C. J. Kin, A.A. Shelton, M. Januszyk, G.C. Gurtner, G. Wernig, M.T. Longaker, Elucidating the fundamental fibrotic processes driving abdominal adhesion formation, Nat. Commun. 11 (1) (2020) 4061.
[39] X. Wang, E.R. Simpson, K.A. Brown, p53: protection against tumor growth beyond effects on cell cycle and apoptosis, Canc. Res. 75 (23) (2015) 5001–5007.
[40] S.S. Mello, L.D. Attardi, Deciphering p53 signaling in tumor suppression, Curr. Opin. Cell Biol. 51 (2018) 65–72.
[41] H. Men, H. Cai, Q. Cheng, W. Zhou, X. Wang, S. Huang, Y. Zheng, L. Cai, The regulatory roles of p53 in cardiovascular health and disease, Cell. Mol. Life Sci. 78 (5) (2021) 2001–2018.
[42] E. Volpe, M. Sambucci, L. Battistini, G. Borsellino, Fas-fas ligand: checkpoint of T cell functions in multiple sclerosis, Front. Immunol. 7 (2016) 382.
[43] F. Item, S. Wueest, V. Lemos, S. Stein, F.C. Lucchini, R. Denzler, M.C. Fisser, T. D. Challa, E. Pirinen, Y. Kim, S. Hemmi, E. Gulbins, A. Gross, L.A. O'Reilly, M. Stoffel, J. Auwerx, D. Konrad, Fas cell surface death receptor controls hepatic lipid metabolism by regulating mitochondrial function, Nat. Commun. 8 (1) (2017) 480.
[44] S.N. Zwicky, D. Stroka, J. Zindel, Sterile injury repair and adhesion formation at serosal surfaces, Front. Immunol. 12 (2021) 684967.
[45] J. Zindel, M. Peiseler, M. Hossain, C. Deppermann, W.Y. Lee, B. Haenni, B. Zuber, J.F. Deniset, B.G.J. Surewaard, D. Candinas, P. Kubes, Primordial GATA6 macrophages function as extravascular platelets in sterile injury, Science 371 (6533) (2021).
[46] M.J. O'Connell, N.C. Walworth, A.M. Carr, The G2-phase DNA-damage checkpoint, Trends Cell Biol. 10 (7) (2000) 296–303.
[47] A. Pal, S. Sengupta, R. Kundu, Tiliacora racemosa leaves induce oxidative stress mediated DNA damage leading to G2/M phase arrest and apoptosis in cervical cancer cells SiHa, J. Ethnopharmacol. 269 (2021) 113686.
[48] A. Harada, N. Sekido, T. Akahoshi, T. Wada, N. Mukaida, K. Matsushima, Essential involvement of interleukin-8 (IL-8) in acute inflammation, J. Leukoc. Biol. 56 (5) (1994) 559–564.
[49] M.E. Hammond, G.R. Lapointe, P.H. Feucht, S. Hilt, C.A. Gallegos, C.A. Gordon, M. A. Giedlin, G. Mullenbach, P. Tekamp-Olson, IL-8 induces neutrophil chemotaxis predominantly via type I IL-8 receptors, J. Immunol. 155 (3) (1995) 1428–1433.
[50] L. Yang, L. Liu, R. Zhang, J. Hong, Y. Wang, J. Wang, J. Zuo, J. Zhang, J. Chen, H. Hao, IL-8 mediates a positive loop connecting increased neutrophil extracellular traps (NETs) and colorectal cancer liver metastasis, J. Canc. 11 (15) (2020) 4384–4396.
[51] A.K. Mehta, D.T. Gracias, M. Croft, TNF activity and T cells, Cytokine 101 (2018) 14–18.
[52] A. Mancusi, S. Piccinelli, A. Velardi, A. Pierini, The effect of TNF-α on regulatory T cell function in graft-versus-host disease, Front. Immunol. 9 (2018) 356.
[53] R. Malaviya, J.D. Laskin, D.L. Laskin, Anti-TNFalpha therapy in inflammatory lung diseases, Pharmacol. Ther. 180 (2017) 90–98.
[54] Z. Yang, Y. Qi, N. Lai, J. Zhang, Z. Chen, M. Liu, W. Zhang, R. Luo, S. Kang, Notch1 signaling in melanoma cells promoted tumor-induced immunosuppression via upregulation of TGF-β1, J. Exp. Clin. Canc. Res. 37 (1) (2018) 1.
[55] H. Ungefroren, Autocrine TGF-β in cancer: review of the literature and caveats in experimental analysis, Int. J. Mol. Sci. 22 (2) (2021).
[56] R. Derynck, S.J. Turley, R.J. Akhurst, TGFβ biology in cancer progression and immunotherapy, Nat. Rev. Clin. Oncol. 18 (1) (2021) 9–34.
[57] G. Visco, [Immunoglobulins], Policlinico Prat 78 (6) (1971) 245–250.
[58] A. Pathak, A. Agrawal, Evolution of C-reactive protein, Front. Immunol. 10 (2019) 943.
[59] N.Y. Elmadhun, A.A. Sabe, A.D. Lassaletta, R.S. Dalal, F.W. Sellke, Effects of alcohol on postoperative adhesion formation in ischemic myocardium and pericardium, Ann. Thorac. Surg. 104 (2) (2017) 545–552.
[60] J.J. Tomasek, G. Gabbiani, B. Hinz, C. Chaponnier, R.A. Brown, Myofibroblasts and mechano-regulation of connective tissue remodelling, Nat. Rev. Mol. Cell Biol. 3 (5) (2002) 349–363.
[61] T.K. Borg, T.A. Baudino, Dynamic interactions between the cellular components of the heart and the extracellular matrix, Pflügers Archiv 462 (1) (2011) 69–74.
[62] M.L. Bochaton-Piallat, G. Gabbiani, B. Hinz, The Myofibroblast in Wound Healing and Fibrosis: Answered and Unanswered Questions, 2016, p. F1000Res, 5.
[63] C.S. Moore, S.J. Crocker, An alternate perspective on the roles of TIMPs and MMPs in pathology, Am. J. Pathol. 180 (1) (2012) 12–16.
[64] H. Atta, M. El-Rehany, E. Roeb, H. Abdel-Ghany, M. Ramzy, S. Gaber, Mutant matrix metalloproteinase-9 reduces postoperative peritoneal adhesions in rats, Int. J. Surg. 26 (2016) 58–63.
[65] N. Cui, M. Hu, R.A. Khalil, Biochemical and biological attributes of matrix metalloproteinases, Prog Mol Biol Transl Sci 147 (2017) 1–73.
[66] X. Peng, E.S. Nelson, J.L. Maiers, K.A. DeMali, New insights into vinculin function and regulation, Int Rev Cell Mol Biol 287 (2011) 191–231.
[67] J.L. Bays, K.A. DeMali, Vinculin in cell-cell and cell-matrix adhesions, Cell. Mol. Life Sci. 74 (16) (2017) 2999–3009.
[68] M.A. Cole, T. Quan, J.J. Voorhees, G.J. Fisher, Extracellular matrix regulation of fibroblast function: redefining our perspective on skin aging, J Cell Commun Signal 12 (1) (2018) 35–43.